# Atmospheric Response to Local Upwelling in the Vicinity of New York–New Jersey Harbor

JULIE PULLEN AND TEDDY HOLT
*Marine Meteorology Division, Naval Research Laboratory, Monterey, California*

ALAN F. BLUMBERG
*Civil, Environmental, and Ocean Engineering, Stevens Institute of Technology, Hoboken, New Jersey*

ROBERT D. BORNSTEIN
*Meteorology Department, San Jose State University, San Jose, California*

(Manuscript received 5 May 2006, in final form 25 September 2006)

ABSTRACT

Multiply nested urbanized mesoscale model [Coupled Ocean–Atmosphere Mesoscale Prediction System (COAMPS)] simulations of the New York–New Jersey metropolitan region are conducted for 4–11 July 2004. The simulations differ only in their specification of sea surface temperatures (SSTs) on nest 4 (1.33-km resolution) and nest 5 (0.44-km resolution). The "control SST" simulation (CONTROL-SST) uses an analyzed SST product, whereas the "New York Harbor Observing and Prediction System (NYHOPS) SST" simulation (NYHOPS-SST) uses hourly SSTs from the NYHOPS model hindcast. Upwelling-favorable (southerly) winds preceding the simulation time period and continuing for much of the first 5 days of the simulation generate cold water adjacent to the New Jersey coast and a cold eddy immediately outside of the harbor in the New York Bight. Both features are prominent in NYHOPS-SST but are not pronounced in CONTROL-SST. The upwelled water has a discernible influence on the overlying atmosphere by cooling near-surface air temperatures by approximately 1°–2°C, slowing the near-surface winds by 15%–20%, and reducing the nocturnal urban heat island effect by up to 1.3°C. At two coastal land-based sites and one overwater station, the wind speed mean bias is systematically reduced in NYHOPS-SST. During a wind shift to northwesterly on day 6 (9 July 2004) the comparatively cooler NYHOPS-SSTs impact the atmosphere over an even broader offshore area than was affected in the mean during the previous 5 days. Hence, air temperature evolution measured at the overwater site is better reproduced in NYHOPS-SST. Interaction of the offshore flow with the cool SSTs in NYHOPS-SST induces internal boundary layer (IBL) formation, sustained and deepened by turbulent kinetic energy advected from adjacent land areas; IBL formation did not occur in CONTROL-SST.

## 1. Introduction

Coastal regions are rendered complex by abrupt topography, shallow bathymetry, irregular coastlines, corrugated cities, discharging rivers, and ocean and atmosphere processes spawned by these boundary features. The dynamics of continental boundary regions are characterized by rapid response times (on the order of hours) associated with, for example, sea-breeze fronts in the atmosphere and upwelling fronts in the ocean. The aim of this study is to accurately simulate surface land and ocean processes in the New York–New Jersey (NY–NJ) area to better understand atmospheric responses to surface forcing. By utilizing a realistic high-resolution urbanized atmospheric model that responds to sea surface temperatures (SSTs) from a high-fidelity ocean model, this work seeks to illuminate aspects of the boundary layer (BL) response to localized upwelled water, which is common in summer.

Along the U.S. West Coast, where the continental shelf is very narrow, upwelling fronts are numerous and have been intensively studied for over 30 yr. Yet only recently has direct evidence for the influence of coastal ocean upwelling on the atmosphere emerged. In the 2001 Coastal Ocean Advances in Shelf Transport

*Corresponding author address:* Julie Pullen, Marine Meteorology Division, Naval Research Laboratory, 7 Grace Hopper Ave., Monterey, CA 93943.
E-mail: pullen@nrlmry.navy.mil

DOI: 10.1175/JAM2511.1

(COAST) observational program the atmosphere was observed to cool by over 1°C through contact with the cold water that upwelled out to about 50 km offshore along central Oregon (Bane et al. 2005). Along the U.S. East Coast in summertime, persistent south (upwelling favorable) winds associated with the Bermuda high pressure system induce coastal surface waters to cool by 1°–4°C, and they remain cooled for days after the cessation of these winds (Glenn et al. 2004). In the shallow coastal waters of the broad NJ shelf, upwelling becomes intensified in several preferred locations or "centers" linked to shallow bathymetry adjacent to river deltas (Glenn et al. 2004; Song et al. 2001). An upwelling center can also form outside the mouth of the NY harbor (in the NY Bight) where the ocean depth is ~20 m. The orientation of southerly/southwesterly winds relative to the coastline also produces upwelling within Long Island Sound, while more westerly winds generate upwelling along the southern coast of Long Island (Neuman 1996).

Runoff from the Hudson River contributes to the spatial heterogeneity of the SST field in the NY–NJ harbor. The river water is typically warmer than offshore waters because of the shallowness of the riverbed, and the Hudson River is at its warmest in July, although its discharge is lowest in July and August. The mean monthly climatological (1946–2004) discharge peak of 824 $m^3 s^{-1}$ occurs in January, while the value for July is only 249 $m^3 s^{-1}$ (Blumberg and Hellweger 2006). The July 2004 discharge of 258 $m^3 s^{-1}$ is indistinguishable from the July climatological average. Last, urban sources like discharge from power plants and combined sewer overflow can introduce anomalous temperature signatures in adjacent waters.

In addition to the SST effects, the NY–NJ region also has a highly developed urban landscape known to generate pronounced urban heat islands (UHIs), whereby the city acts as a nocturnal heat reservoir relative to the surrounding rural environments. The UHI builds up from sunset to midnight (Oke and Maxwell 1975) as rural areas cool rapidly, while urban areas cool less because of the release of their stored solar energy (low-latitude cities) or their anthropogenic heat production (high-latitude cities). After midnight, both areas cool at about the same rate, and thus the heat island magnitude is maintained until sunrise. In the New York City (NYC) metropolitan area, the UHI is strongest near the surface (2°–5°C; Bornstein 1968; Gedzelman et al. 2003). Urban-induced atmospheric circulations are typically on the city-size scale, but they can have significant impacts on the mesoscale dynamics. For example, winds accelerate and converge into cities during strong UHI periods and decelerate and diverge around cities in weak UHI periods (Bornstein and Johnson 1977). Synoptic and sea-breeze frontal passage speeds can also be frictionally retarded by 50% as they approach NYC (Loose and Bornstein 1977; Bornstein and Thompson 1981). Urban heating also distorts near-surface temperatures as sea-breeze fronts pass NYC (Novak and Colle 2006). Summer thunderstorms have been observed to either initiate over NYC during otherwise clear-sky, low-wind, UHI-induced convergence conditions or split and go around the city during cloudy, windy, non-UHI conditions in response to an urban-induced barrier effect (Bornstein and LeRoy 1990).

Sharp discontinuities in surface properties (e.g., rural-to-urban roughness or land-to-ocean temperature fronts) can cause atmospheric internal boundary layers (IBLs) to form (Garratt 1990). Because of complexities inherent in coastal regimes, the study of IBLs has typically been approached by the use of idealized or simplified numerical simulations (Skyllingstad et al. 2005; Smedman et al. 1997), as opposed to the realistic data-assimilating simulations presented here.

The impact of cold upwelled water on near-surface air properties in the NY–NJ harbor region, as well as on formation mechanisms for IBLs, are investigated using realistic finescale simulations of the NY–NJ metropolitan area. The time period of interest is July 2004, when the NJ shelf presented classic signatures of coastal upwelling. In section 2 the modeling system is described. Section 3 describes the synoptic scenario for the simulation time period. In sections 4 and 5, observations from the ocean and atmosphere are compared with simulation results. The focus is on the spatially heterogeneous aspects of the atmospheric response during upwelling-favorable versus offshore winds. The paper concludes with a discussion of the results in section 6.

## 2. Modeling system

### *a. Description*

The nonhydrostatic Coupled Ocean–Atmosphere Mesoscale Prediction System (COAMPS) data-assimilating model (Hodur 1997) is configured for a U.S. East Coast five-nest domain with resolutions of 36, 12, 4, 1.33, and 0.444 km, focused on the island of Manhattan (maximum width of 3.7 km and length of 21 km) and adjacent waters (Fig. 1). The model utilizes 60 vertical sigma levels, with 30 levels in the lowest 1200 m (and 13 in the lowest 100 m) to allow for greater resolution of BL processes. Simulations are conducted for 1 week (4–11 July 2004). The first simulation starts at 0000 UTC 4 July and uses initial fields interpolated from the U.S. Navy's Operational Global Atmospheric

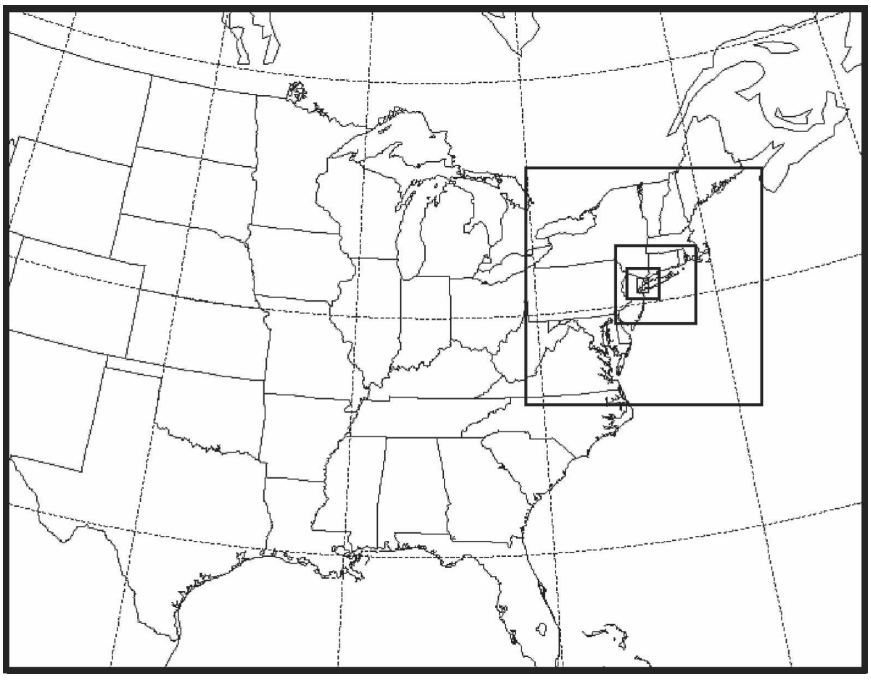

FIG. 1. COAMPS nest domains 1 (36 km), 2 (12 km), 3 (4 km), 4 (1.33 km), and 5 (0.444 km).

Prediction System (NOGAPS) 1° model, and all subsequent forecast cycles use the previous COAMPS forecast as initial conditions. At the beginning of each assimilation cycle (every 12 h), a 3D multivariate optimum interpolation (MVOI), using quality-controlled data from radiosondes, surface stations, aircraft, and satellites, is conducted (Hodur 1997). Subsequently, 24-h forecasts are run forward. The outermost 36-km nest receives boundary conditions from NOGAPS at a 6-h interval. Both BL and subgrid-scale turbulence processes in COAMPS are represented by a turbulent kinetic energy (TKE) scheme following Mellor and Yamada (1982), with surface layer parameterization after Louis et al. (1982). The radiation scheme is that of Harshvardhan et al. (1987). Moist processes on the 36- and 12-km nests are simulated using a modified Kain and Fritsch (1993) cumulus parameterization, but are treated explicitly on nests 3, 4, and 5, with a modified Rutledge and Hobbs (1983) and Khairoutdinov and Kogan (2000) moist physics parameterization that includes graupel (see more details online at http://www.nrlmry.navy.mil/coamps-web/web/home/).

### b. Urban parameterization

To represent urban effects on mesoscale processes, an urban canopy parameterization (UCP) is used on nests 4 and 5. In COAMPS, the enhanced UCP formulation of Chin et al. (2005), including a rooftop surface energy equation, builds on the original work of Brown and Williams (1998). The urban canopy acts as a friction source and is represented via modified aerodynamic drag in the momentum equations. Thermal effects are included through a modified thermodynamic equation that considers the heat fluxes from rooftop, street, and building walls. The urban canopy is also treated as a source of turbulence production to account for turbulence wake generation of TKE. The addition of a rooftop surface energy equation enables the UCP to exhibit a more reasonable diurnal cycle of heat island values (Chin et al. 2005).

The UCP requires several input parameters to describe urban environment morphology. The distinction between urban (on nests 4 and 5) and nonurban regions is determined using the U.S. Geological Survey (USGS) 24-category 30-s dataset. For the current simulations, it is enhanced using a gridded 250-m-resolution database for the NY–NJ region (Burian et al. 2005). This high-resolution database provides building characteristics, such as mean height, plan-area fraction, and sky-view factor. The tallest buildings are generally concentrated in midtown and lower Manhattan (Fig. 2), with a maximum building height of 200 m. Table 1 summarizes UCP values used for nests 4 and 5, as interpolated from Burian et al. (2005) and following Brown and Williams (1998). Holt and Pullen (2007) describe

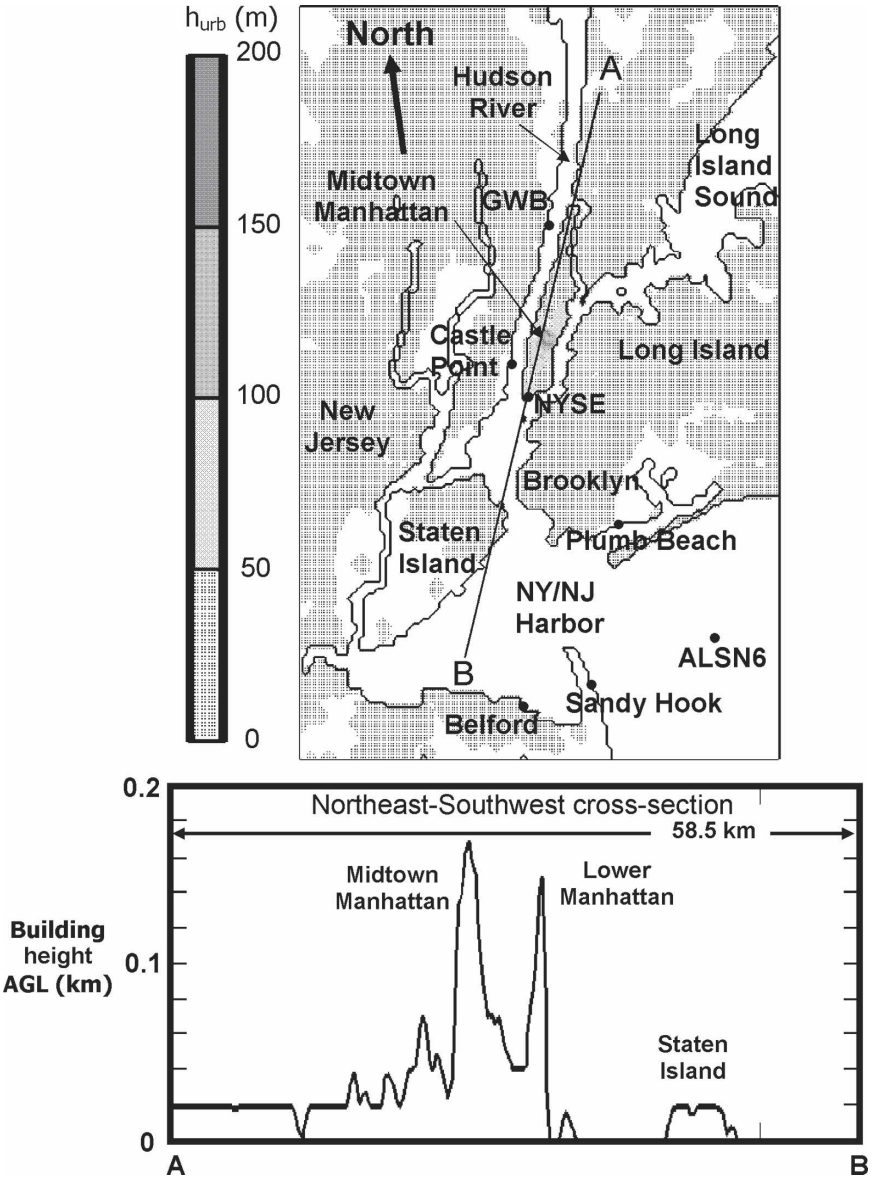


FIG. 2. COAMPS nest-5 building heights (m) used in the (top) urban parameterization and (bottom) along-northeast–southwest cross section A–B, with points of interest discussed in text.

the UCP in more detail and present comparisons with airport and other land-based observations.

*c. Sea surface temperature specification*

Two COAMPS simulations are performed using different SST specifications. For both simulations, nests 1–3 use analyzed SSTs, which are derived from an optimum interpolation of available satellite and in situ data as implemented in the standard COAMPS infrastructure and used in operational and research applications (Chen et al. 2003). When data are scarce, the analyzed SSTs tend to be smooth, and this is particularly true when the domain is small. For the control simulation (CONTROL-SST), analyzed SSTs are also used for nests 4 and 5, while for the sensitivity simulation [New York Harbor Observing and Prediction System (NYHOPS)-SST] SSTs are interpolated to COAMPS nests 4 and 5 from hourly NYHOPS ocean model hindcast fields.

The NYHOPS modeling system is based on a shallow-water version of the Princeton Ocean Model (POM). It is a 3D, time-dependent, estuarine and

TABLE 1. Description of urban canopy parameters for nests 4 and 5.

| | Building height (m) | Urban fraction | Roof fraction | Anthropogenic heating (W $m^{-2}$) | Urban drag (N $m^{-2}$) |
|---|---|---|---|---|---|
| Manhattan and surrounding urban regions | Burian et al. (2005); see Fig. 1. | Burian et al. (2005) | Burian et al. (2005) | 50 | Building height × 0.0005 |
| Suburban regions | 12 | 0.2 | 0.1 | 20 | 0.01 |

coastal circulation model developed by Blumberg and Mellor (1987) that incorporates the Mellor–Yamada 2.5-level turbulent closure model to provide realistic parameterization of vertical mixing processes. The spatial extent of the NYHOPS domain covers the NY–NJ harbor and extends beyond to include the Hudson River and Estuary up to the Troy Dam, all of Long Island Sound, and the NY Bight out to the continental shelf break. Its orthogonal–curvilinear coordinate system resolves the complex and irregular shoreline of the NY–NJ harbor–NY Bight region. The resolution of the computational grid varies from 500 m in the rivers to about 25 km in the NY Bight. The depth of the water column varies from approximately 100 to less than 2 m, and the model uses 11 vertical sigma-coordinate levels (Blumberg et al. 1999).

Near-real-time measurements of water level, meteorological forcing [National Centers for Environmental Prediction (NCEP) 12-km-resolution Eta Model], spatially and temporally varying surface heat flux, and freshwater fluxes from 43 rivers (measured at USGS gauges) and 110 wastewater treatment plants (using data from the Interstate Sanitation Commission) are used as model forcing. Salinity and temperature boundary conditions located far offshore are derived from climatological data. Each day NYHOPS produces a 24-h hindcast/nowcast and a 48-h forecast of the physical state of the marine environment (Bruno and Blumberg 2004). Water level, currents, temperature, and salinity are predicted in a system in operation since late 2003.

NYHOPS has been calibrated and validated for two annual cycles (i.e., 1 October 1994–30 September 1995 and 1 October 1988–30 September 1989) by Blumberg et al. (1999). Results were compared with water levels at 14 stations, currents at 6 stations, and temperature and salinity at 35 stations. Mean errors in predicted elevations and currents were less than 10% and 15%, respectively. Correlation coefficients for salinity and temperature were as high as 0.86 and 1.0, respectively.

In a more recent exercise, model hindcast/forecast skill assessment has been quantified for the entire year 2004 at 12 stations (Fan et al. 2006). At most stations, errors in computed water levels were less than 8.5% of the local tidal range, while correlations between data and model results exceeded 94%; model performance for salinity and temperature were also very good. Vertical salinity stratification and its temporal variations in the different regions in the model domain were accurately reproduced. Correlation coefficients ranged at various stations from 0.64 to 0.79 for salinity, and typically exceeded 0.96 at all stations for temperature. NYHOPS data and model products are available in real time (online at http://www.stevens.edu/maritimeforecast).

## 3. Synoptic setting and model evaluation

Two dominant synoptic settings during the 4–11 July 2004 time period of the numerical simulations impacted low-level flows in the NY–NJ area of interest. The first was characterized by generally quiescent atmospheric forcing with a low-level southerly (upwelling favorable) flow. This general pattern was evident over the U.S. East Coast from 28 June 2004, extending through the initial time period of the study (0000 UTC 4 July) until approximately 0000 UTC 9 July. Figure 3a shows the 1200 UTC 5 July low-level conditions typical of this upwelling-favorable regime. A low pressure area is situated well to the west-northwest of the region, while high pressure is located well offshore of the East Coast, resulting in southerly flow and regions of coastal low-level convergence. An upper-level ridge is generally aligned along or just offshore of the East Coast, with little upper-level temperature advection (Fig. 3b). A brief break in the pattern, from approximately 0600 UTC 6 July to 1200 UTC 7 July, occurred when a frontal system rapidly propagated through the NY–NJ region; however, the low-level flow quickly returned to southerly and persisted until approximately 0000 UTC 9 July. SST response to such a brief break (~1 day) in upwelling favorable forcing is typically not appreciable.

The second synoptic setting occurred at approximately 0000 UTC 9 July, when persistent low-level northwesterly (offshore) flow was evident over the NY–NJ area. The 1200 UTC 9 July low-level conditions (Fig. 3c) show flow typical of this regime, with the offshore flow associated with the low pressure center offshore of Maine and the front stretching southeastward to the North Carolina coast. The associated upper-level

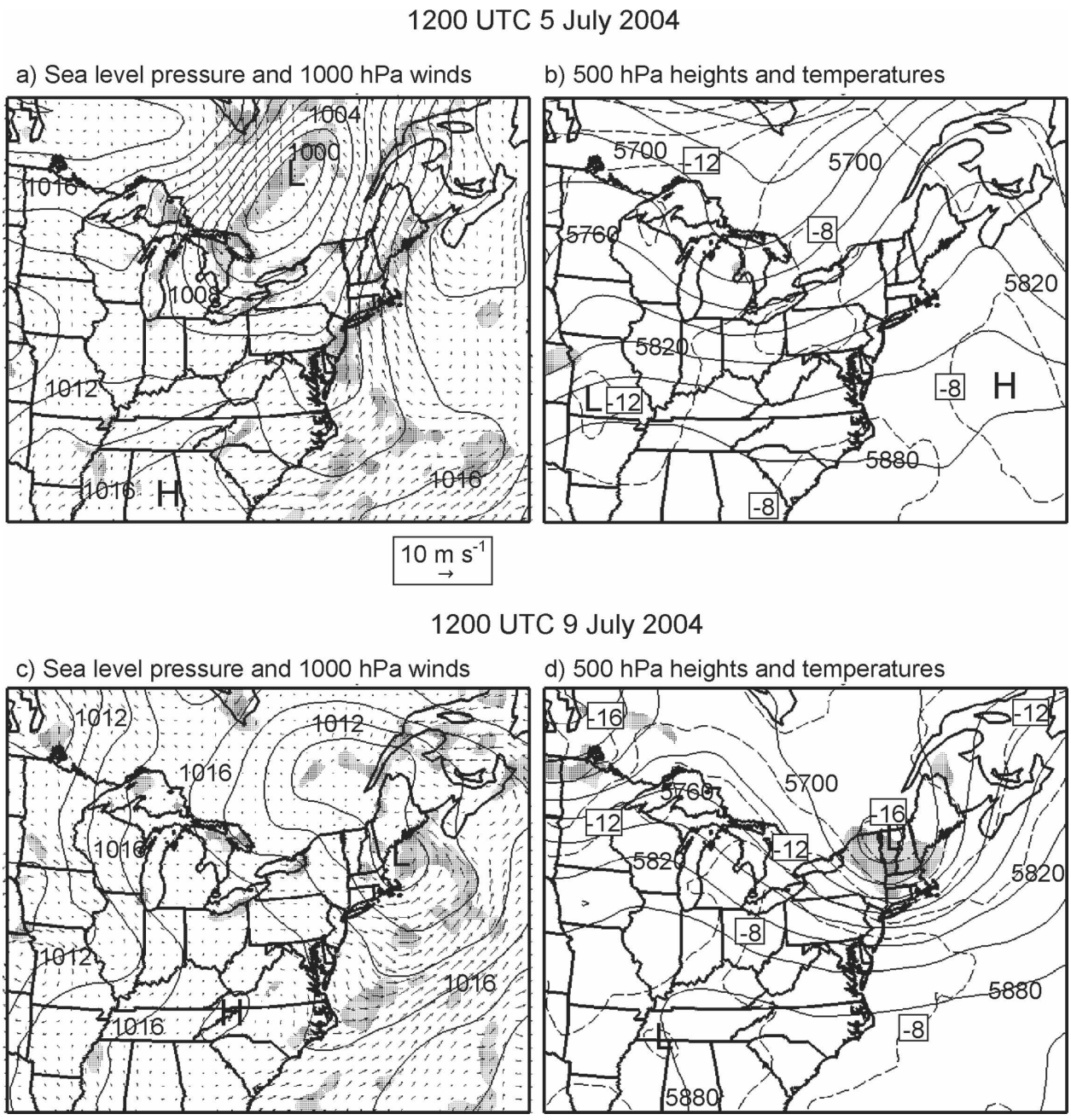


FIG. 3. COAMPS nest-1 (36 km) analyses at 1200 UTC 5 Jul 2004 for subarea of the eastern United States for (a) sea level pressure (solid line, interval of 2 hPa), 1000-hPa winds (arrows at every other grid point), and regions of horizontal convergence $>2.0 \times 10^{-5}$ $s^{-1}$ (shaded) and (b) 500-hPa geopotential heights (solid line, interval of 30 m), temperatures (dashed line, interval of 2°C), and regions of absolute vorticity $>2.0 \times 10^{-4}$ $s^{-1}$ (shaded). (c), (d) Same as (a) and (b), but for 1200 UTC 9 Jul 2004.

trough is well defined, with a significant vorticity maximum over upper New England (Fig. 3d). The trough is generally slow to propagate off the East Coast, and thus low-level northwesterly flow remains along the NY–NJ coast through the end of the simulation period (at 0000 UTC 11 July).

Observed and model forecast time series at the National Oceanic and Atmospheric Administration/National Data Buoy Center (NOAA/NDBC) station at the Ambrose light tower (ALSN6; 40.4667°N, −73.90°E, 29-m sensor height, and station location shown in Fig. 2) further illustrates the differing low-level atmospheric characteristics for the upwelling versus offshore regimes (Fig. 4). The COAMPS time series represent

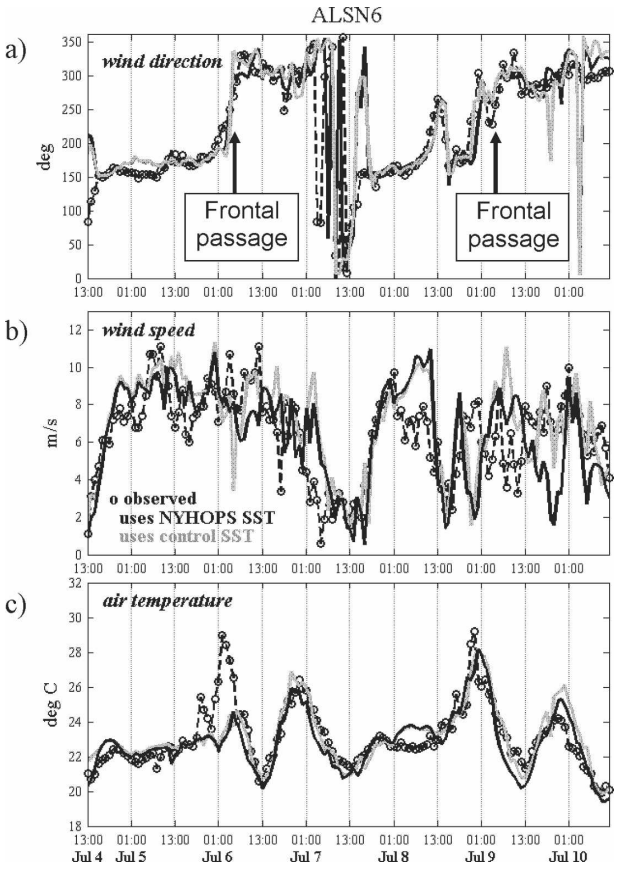


FIG. 4. COAMPS 27-m-elevation results for CONTROL-SST (gray) and NYHOPS-SST (black) and 29-m observations (circles) at ALSN6 for time period of 1300 UTC 4 Jul–1200 UTC 10 Jul 2004 for (a) wind direction (°), (b) wind speed (m $s^{-1}$), and (c) air temperature (°C); observed frontal passage is indicated by vertical arrow.

nest-5 fields extracted at the observation site at the nearest model vertical sigma level (27 m) for forecast hours 1–12 of each data assimilation cycle. The observed times of frontal passage, indicated by the vertical arrow in Fig. 4a, are based primarily on shifts in wind direction from a more southerly component to a northerly component. The first observed passage at approximately 0600 UTC 6 July marks a clear shift in wind direction over a period of only several hours, and the second passage at approximately 0600 UTC 9 July occurs over a longer time period (~6–12 h).

Several wind shifts occur from 1300 UTC 8 July to 0600 UTC 9 July, and not until approximately 1200 UTC 9 July does the low-level flow become steady from the northwest. For the observed wind speed, the degree of variability in the prefrontal versus postfrontal flow is not large, with speeds typically ranging from 6 to 10 m $s^{-1}$ (Fig. 4b). The exception occurs from approximately 0300 to 1500 UTC 7 July, in association with a weakened pressure gradient between frontal systems and with light and variable winds. Observed temperatures at ALSN6 show nearly identical features for the two pre- and postfrontal regimes (Fig. 4c).

For the prefrontal regimes (1200 UTC 4 July–0000 UTC 6 July and 0000 UTC 8 July–0000 UTC 9 July), temperatures are approximately constant (~22.0°–22.5°C) until 0000–0100 UTC, when they increase to ~29°C as winds shift from southerly to northwesterly. As this wind shift occurs over several hours, it results in significant warm-air advection from the land located to the southwest of ALSN6 (which has warmed to over 30°C during the daytime). For the two postfrontal regimes (1200 UTC 6 July–0600 UTC 7 July and 1200 UTC 9 July–1200 UTC 10 July), temperatures initially decrease to approximately 20°C when the front passes, increase to approximately 24°–26°C in conjunction with the northwesterly warm-air advection from the land, and then decrease to approximately 20°–21°C at night.

Both model simulations generally agree well with the observed wind direction, speed, and air temperature throughout the entire period, resulting from several factors, including data assimilation, quasi-steady synoptic forcing, and relatively short (12 h) forecast periods. The 6°–7°C increase in observed air temperature from 0000 to 0100 UTC 6 July, associated with the southwesterly warm-air advection from the land, is not, however, forecasted in either simulation, perhaps because of the slight timing error in the COAMPS forecasts of frontal passage. Note that the model wind shift associated with the frontal passage occurs 2–3 h later than observed, at approximately 0400 UTC (0000 LT). The timing error is crucial, because by 0400 UTC the land has significantly cooled and the associated warm-air advection is reduced in the simulations. Warm-air advection is evident in the model simulations (note the slight increase from approximately 22°C at 0100 UTC 6 July to 24°C at 0400 UTC), but is much less than observed. In contrast, the warm-air advection, and hence the low-level temperatures, associated with the second prefrontal period (0000–0100 UTC 9 July) is modeled much better, because of a more accurate timing prediction of the frontal passage.

## 4. SST dynamics

Because of the persistence of low-level southerly winds over the NY–NJ area from as early as 28 June, upwelling-favorable conditions existed for more than 10 days. Satellite SST observations on 9 July show anomalously cold water outside the harbor in the NY Bight in association with an eddy signature (Fig. 5a). The SSTs on nest 5 for both CONTROL-SST and NYHOPS-SST indicate colder waters in this region

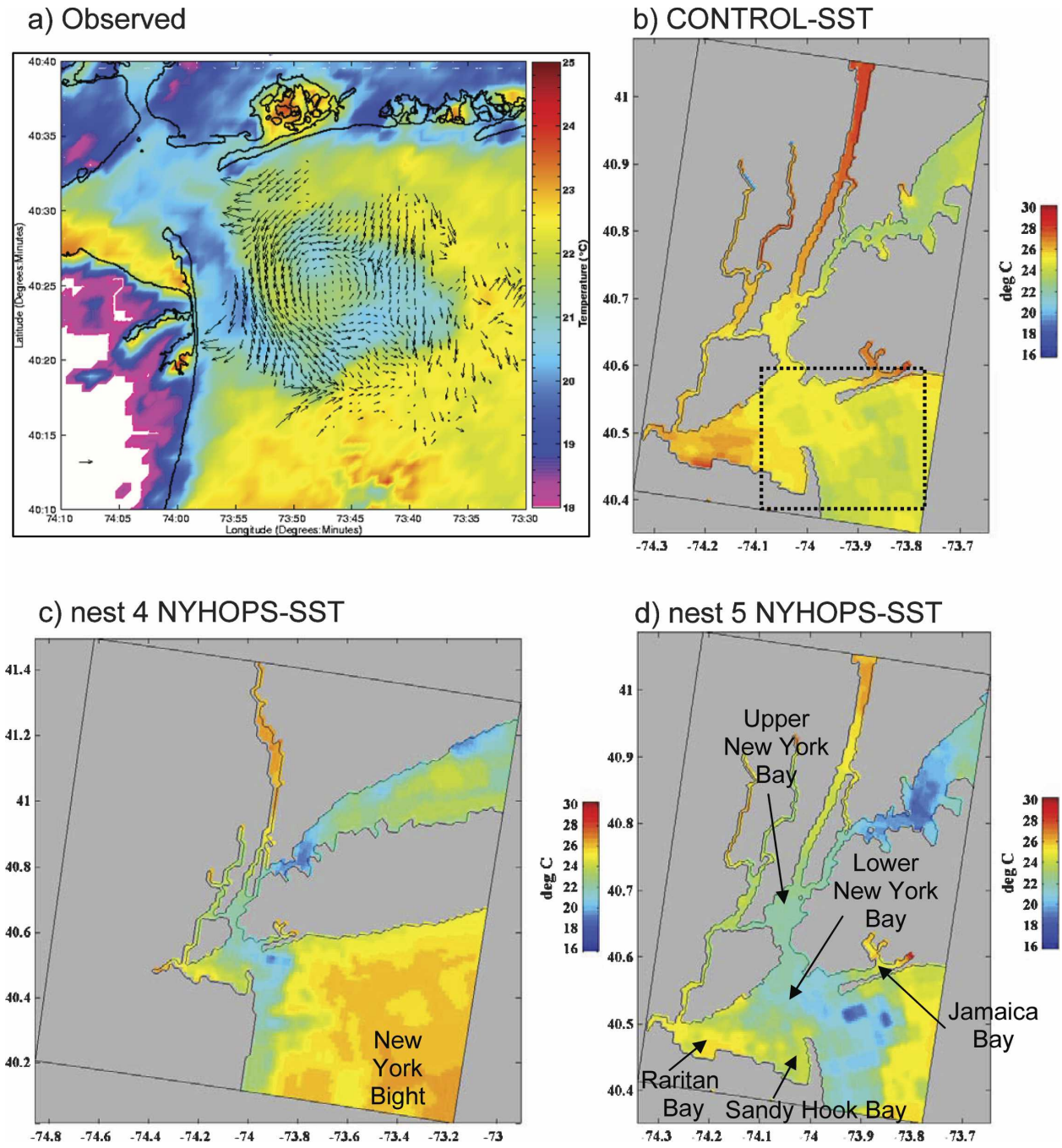


FIG. 5. (a) Advanced Very High Resolution Radiometer satellite image of SST and coincident ocean surface radar velocity vectors from 0800 UTC 9 Jul 2004 (courtesy of S. Glenn, Rutgers University) for approximate region shown by box in (b). (b) Analyzed SST in nest-5 CONTROL-SST simulation; (c) NYHOPS model SST in nest-4 NYHOPS-SST; and (d) same as (c), but for nest 5. Oceanic points of interest discussed in text are shown in (c) and (d).

(Figs. 5b,d), although NYHOPS-SST is ~4°C cooler than CONTROL-SST, in accord with the satellite data. Cool waters are also found in NYHOPS-SST and in the satellite SST field in the lower and upper NY bays, but not in CONTROL-SST. Large (~4°C) cold-to-warm temperature gradients between the coastal waters and inshore waters (e.g., resulting from the shallow, warm inshore waters of Raritan and Jamaica Bays) are seen in the satellite field and are well simulated in NYHOPS-SST. The nest-4 (1.33-km resolution)

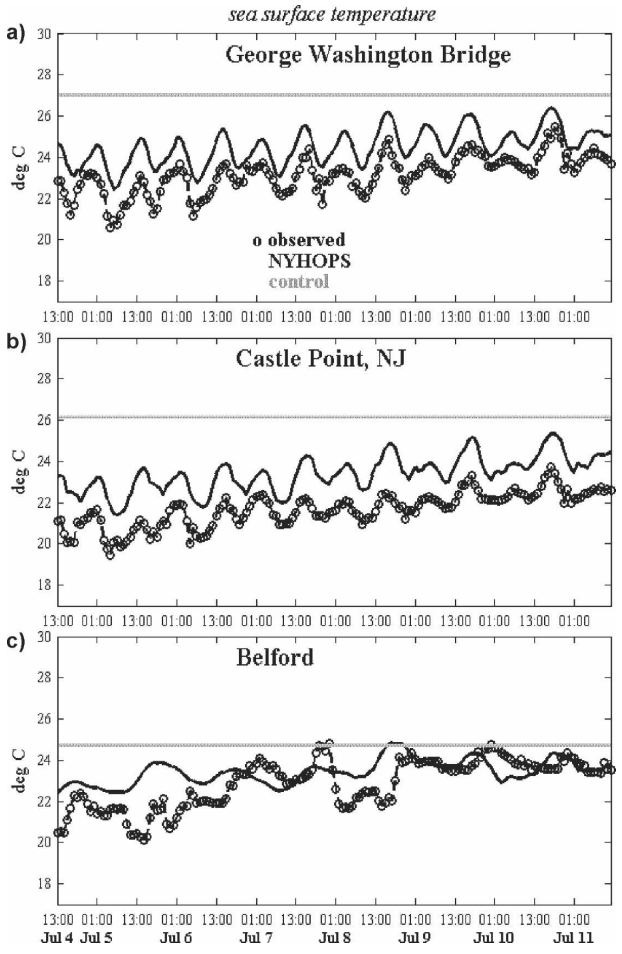


FIG. 6. Observed (circles), CONTROL-SST (gray line), and NYHOPS-SST (black line) sea surface temperature (°C) for 1300 UTC 4 Jul–1200 UTC 11 Jul 2004 (7 days) at (a) GWB, (b) Castle Point, and (c) Belford.

NYHOPS-SST (Fig. 5c) southward extension of cold water along the NJ coast, and the cool temperatures in the Long Island Sound, are hallmarks of upwelling. By contrast, the CONTROL-SST does not contain strong signatures of upwelled water.

A transient eddy feature, often evident in surface radar fields that map ocean currents (arrows in Fig. 5a), is believed to be strongly tidally influenced. Its relation to forcing factors, including the Hudson River discharge rate, is currently under investigation. Generally, NYHOPS model ocean velocities agree with radar-measured surface currents in magnitude and direction for a wide range of flow conditions (S. Glenn and A. Blumberg 2006, personal communication).

Three sites with in situ temperature measurements are available for comparison with model SSTs. Figure 6 illustrates such comparisons at Belford, New Jersey (40.4339°N, −74.0793°E), Castle Point, New Jersey (40.7425°N, −74.0247°E), and the George Washington Bridge (GWB; 40.8593°N, −73.9547°E; locations given in Fig. 2). SSTs in CONTROL-SST are not updated during the simulation because of a lack of accessible telemetered data in the vicinity (thereby effectively fixing analyzed SSTs at climatological values), whereas NYHOPS-SST uses model-derived hourly SSTs. The observations and NYHOPS-SST both display a several-degree warming trend over the 7-day period at all stations.

The observed SST gradient between the coastal ocean (cold waters in satellite image of Fig. 5) and estuary (progressively warmer upriver) is simulated well by NYHOPS-SST, as seen in results from the Castle Point and GWB sites. The observed/NYHOPS mean SSTs at GWB and Castle Point are (22.87°/24.48°C) and (21.67°/23.37°C), respectively, representing a greater-than-1°C mean SST gradient between the stations. This gradient in the presence of the strong harbor tidal currents leads to tidal time-scale (12.42 h) temperature oscillations of 3°C, which are clearly shown in NYHOPS-SSTs at both sites. Those at GWB have a mean bias (MB) of 1.33°C and RMSE of 1.39°C, whereas the CONTROL-SST values are 3.89° and 4.00°C, respectively. Castle Point NYHOPS-SSTs have an MB of 1.70°C and RMSE of 1.76°C, whereas the CONTROL-SST values are 4.50° and 4.58°C, respectively.

The Belford site is more difficult to simulate in terms of the temporal excursions in SST, because it is located in an area with little spatial gradient, is isolated from the main estuarine circulation, and has little exchange with the coastal ocean and estuary. Initially, NYHOPS-SST is too warm (~2°C); however, the initial error disappears by the end of the period (1200 UTC 11 July), when both NYHOPS-SST and the observations are approximately 24°C. At Belford NYHOPS-SST has an MB of 0.55°C and RMSE of 1.21°C, whereas the CONTROL-SST has a constant SST of 24.73°C, resulting in an MB and RMSE of 1.85° and 2.20°C, respectively.

It is apparent that NYHOPS-SST provides a reasonable proxy for in situ ocean and estuary temperature evolution, because the three sites where observations exist have relatively low MB and RMSE. Furthermore, NYHOPS-SST has a much lower MB and RMSE than does CONTROL-SST at all sites.

## 5. Atmospheric response

### *a. Upwelling regime (4–9 July 2004)*

During the 5 days of 1300 UTC 4 July–1200 UTC 9 July (using model forecast hours 1–12), mean 10-m

winds are generally southerly over the nest-5 domain in both CONTROL-SST and NYHOPS-SST, with a more southwesterly orientation over the northern and western portions of the domain (Fig. 7). Speeds are generally stronger over water in both simulations, resulting from reduced surface roughness as compared with land; however, the mean speed is reduced by 15%–20% over most water areas in NYHOPS-SST. The slowing of near-surface winds over cool SSTs is commonly observed in oceanic regions, in both in situ and satellite observations (Chelton et al. 2004). For instance, Vickers and Mahrt (2004) used 10-m-high aircraft flight data to show that SST decreases of 1°–2°C lead to wind speed reductions of approximately 4%, but substantial spread exists in speed responses because of increased sampling errors in stable conditions. Incident surface winds have also been seen to decelerate in the eastern equatorial Pacific as the BL stabilizes above cold pool waters (Chelton et al. 2001). Hallmarks of this process include reduced mixing and a more stabilized BL that serves to decelerate the flow by confining the surface drag effect to a shallower layer.

In both simulations wind speeds are more variable over water than over land, but standard deviations are reduced in NYHOPS-SST over regions of cool SST, when compared with CONTROL-SST. Of note is the reduced wind speed mean and standard deviation in urban areas, especially Manhattan and Brooklyn, in both simulations resulting from the UCP. Patterns of difference for 2-m air temperature mean and standard deviations are similar to the wind results, with mean air temperatures more than 1°C cooler over colder regions of SST in NYHOPS-SST (Fig. 8). Wind speed and air temperature effects resulting from the more spatially variable SST in NYHOPS-SST extend over much of the land surface of the nest-5 domain; however, magnitude differences over land are very small. For instance, within 10 km of the coast, the wind speed difference is less than $-0.25$ m s$^{-1}$ (Fig. 7b) and the air temperature difference is less than $-0.25$°C (Fig. 8b).

Holt and Pullen (2007) present an evaluation of model results using an extensive set of land-based stations, while the current work focuses on coastal and overwater locations. Several in situ coastal meteorological stations in the area are available for evaluating the model simulations, including two coastal stations operated by Weatherflow (Plumb Beach: 40.584°N, −73.931°E, with 20-m sensor height; and Sandy Hook: 40.44°N, −73.987°E, with 15-m sensor height) and the NOAA/NDBC station at the Ambrose light tower (Fig. 2). The Plumb Beach and Sandy Hook locations are categorized as nonurban (Fig. 2). Unfortunately, none of the stations are situated in the regions of elevated differences between the simulation results. Nonetheless, a comparison of the time series does provide a quantitative assessment of overall model skill. COAMPS nest-5 model fields were extracted at the measurement site at the nearest vertical sigma level for forecast hours 1–12 of each data assimilation cycle to construct a 5-day model time series for 1300 UTC 4 July–1200 UTC 9 July. To correspond with the observation heights, model heights of 27, 21, and 15 m are used for ALSN6, Plumb Beach, and Sandy Hook, respectively.

Statistics are computed to quantify differences between the model simulations at the three sites (Table 2), with ALSN6 showing the largest mean and standard deviation of all stations in both the observation and model simulations. The ALSN6 site also has the greatest correspondence between observed and modeled winds, as measured by the correlation coefficients. The Sandy Hook observed time series displays more variability than in either simulation, but the variability at Plumb Beach is overestimated by both simulations. Overall, the model agreement is good at two stations (ALSN6 and Sandy Hook) and poorer at the more secluded site (Plumb Beach), which has the weakest observed mean and standard deviation.

The agreement of both simulations with the observations is respectable, given the complexity of the flow in the region; however, the mean winds at ALSN6 are weaker in NYHOPS-SST, which leads to a somewhat reduced MB relative to CONTROL-SST. The MB of NYHOPS-SST is similarly reduced at the coastal Plumb Beach and Sandy Hook sites. A slight reduction in RMSE exists at all sites for NYHOPS-SST, when compared with CONTROL-SST. By these metrics, NYHOPS-SST produces more skillful forecasts than does CONTROL-SST at all three measured sites.

Differences in the wind field during the 5-day period of generally upwelling-favorable winds are separated into daytime and nighttime periods to examine diurnal effects of SST differences (Fig. 9). In both simulations, mean nighttime winds (0100–1200 UTC, or 2100–0800 LT) are weaker and more disorganized over land, generally larger over water, and more southwesterly in orientation than mean daytime winds (1300–0000 UTC, or 0900–2000 LT). Also, in both simulations, mean daytime winds are oriented southeasterly in the harbor area, consistent with the sea-breeze direction in the southern portion of the domain. During this time, steady synoptically forced low-level southerly flow reinforces the sea breeze in this area, while other sea-breeze fronts typically exist elsewhere (e.g., the Long Island sea-breeze front penetrates from the east), lead-

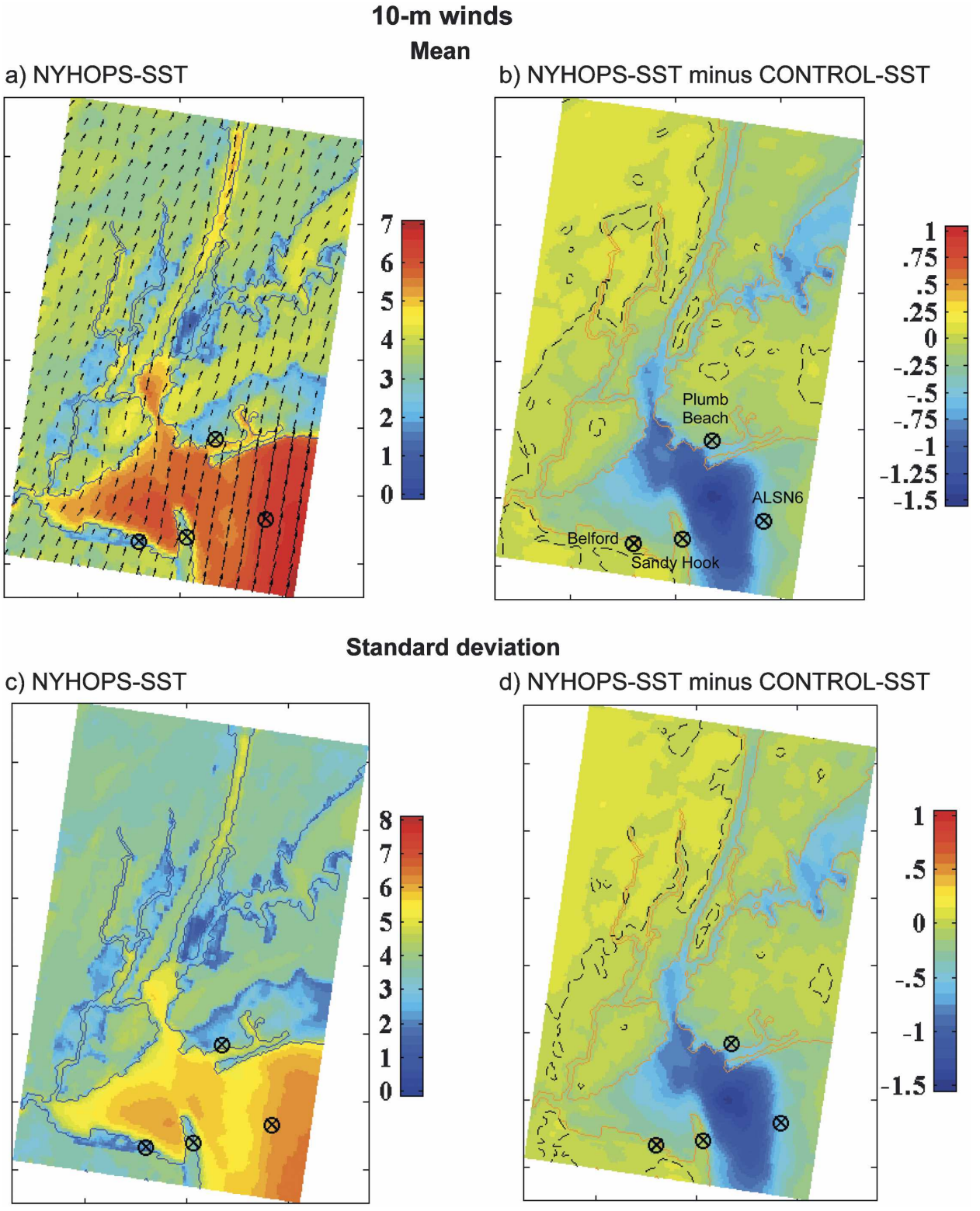


FIG. 7. COAMPS nest-5 1300 UTC 4 Jul–1200 UTC 9 Jul 2004 mean 10-m winds (m $s^{-1}$) for (a) NYHOPS-SST and (b) NYHOPS-SST minus CONTROL-SST, and standard deviation (m $s^{-1}$) for (c) NYHOPS-SST and (d) NYHOPS-SST minus CONTROL-SST. Wind vectors are shown for every 6th grid point. Zero contour is dashed in difference fields, and measurement sites used in model evaluation are shown in (b).

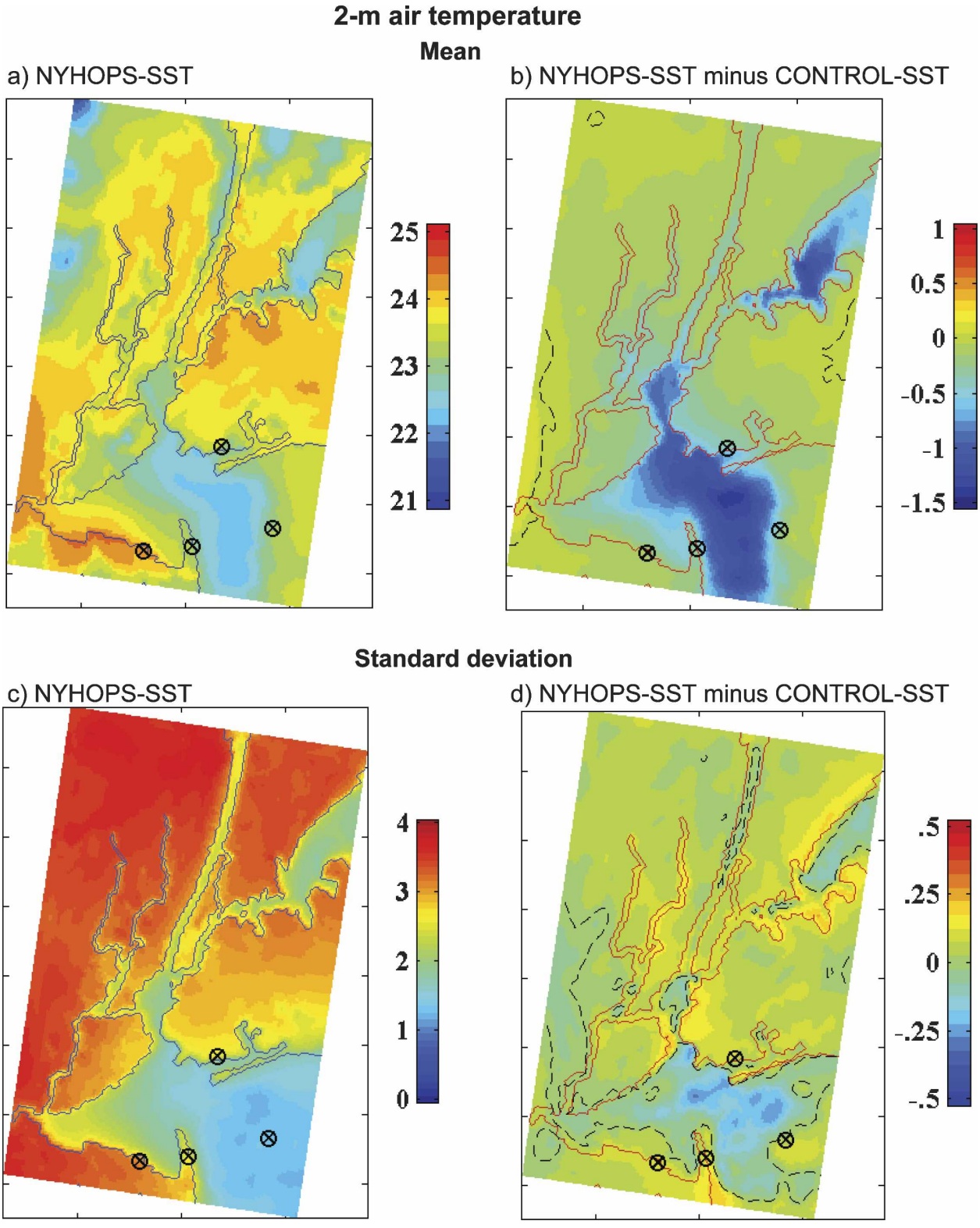


FIG. 8. Same as Fig. 7, but for 2-m air temperature (°C).

TABLE 2. Modeled and observed wind speed statistics and comparison statistics (m $s^{-1}$) for 1300 UTC 4 Jul–1200 UTC 9 Jul 2004 (five days). Here, *N* is number in sample and CC is correlation coefficient.

| | *N* | Mean | Std dev | MB | RMSE | CC |
|---|---|---|---|---|---|---|
| Plumb Beach | | | | | | |
| Observed | 120 | 2.99 | 1.35 | | | |
| CONTROL-SST | 120 | 5.15 | 1.77 | 2.16 | 2.79 | 0.38 |
| NYHOPS-SST | 120 | 4.89 | 1.60 | 1.90 | 2.50 | 0.39 |
| Sandy Hook | | | | | | |
| Observed | 120 | 4.56 | 2.01 | | | |
| CONTROL-SST | 120 | 4.94 | 1.55 | 0.38 | 1.86 | 0.49 |
| NYHOPS-SST | 120 | 4.72 | 1.54 | 0.16 | 1.75 | 0.54 |
| ALSN6 | | | | | | |
| Observed | 120 | 6.38 | 2.43 | | | |
| CONTROL-SST | 120 | 7.18 | 2.55 | 0.80 | 2.28 | 0.63 |
| NYHOPS-SST | 120 | 6.80 | 2.64 | 0.42 | 2.25 | 0.62 |

ing to the complicated frontal evolution in the NY–NJ area reported by Novak and Colle (2006). Differences between simulations are most pronounced at nighttime, when winds are slower in NYHOPS-SST relative to CONTROL-SST in virtually all overwater areas. In particular, the upper NY bay and Long Island Sound winds are now substantially weaker (by over 1.5 m $s^{-1}$) in the NYHOPS-SST nighttime mean (Fig. 9d) when compared with the daytime (Fig. 9b) and overall (Fig. 7b) mean differences. The relatively weaker winds at night for NYHOPS-SST are likely associated with the cooler nighttime SSTs relative to those of CONTROL-SST, which also affect nocturnal air temperatures by cooling the air over 1.5°C in NYHOPS-SST relative to CONTROL-SST (Figs. 10a,b) .

The nocturnal UHI is prevalent in both model simulations. The Manhattan region is generally warmer at night than the surrounding more rural regions (Figs. 10 a,b). Gedzelman et al. (2003) found a typical summertime UHI effect of 4°C from hourly records using an "urban" average of four scattered regional airport stations and a "rural" average of four sites located 50 km inland. They documented smaller UHI values for southeasterly (sea breeze) winds and noted that the sea breezes could delay UHI onset by several hours. The modeled UHI effect is similarly calculated for both simulations, but using a somewhat smaller geographical range. For a site in lower Manhattan (NYSE in Fig. 2) and a rural site in the northwest corner of the domain situated about 20 km west of Manhattan (the asterisks in Fig. 10), maximum nocturnal urban–rural 2-m air temperature differences occur at 0300 UTC 9 July (2300 LT 8 July) and are approximately 5°C in both simulations (Fig. 10c), in agreement with Oke and Maxwell (1975) and Gedzelman et al. (2003). The reduced UHI in the early hours of 6 July is likely a result of the frontal passage displacing the UHI.

Over the 5-day period, the mean nocturnal urban–rural air temperature difference is 2.9°C for CONTROL-SST and 2.4°C for NYHOPS-SST. Both estimates are within the range observed by Gedzelman et al. (2003) for winds from the southern quadrant (~2.5°–3°C). The maximum hourly difference between the UHI in the two simulations is 1.34°C. Thus, the cooler SSTs in NYHOPS-SST reduce the modeled UHI effect by 0.5°C in the mean, but the impact is almost 3 times that during several nights.

### *b. Offshore regime (9–11 July 2004)*

With the change in synoptic flow on 9 July, mean 10-m winds (1300 UTC 9 July through 1200 UTC 10 July) shifted to northwesterly for this offshore regime (Fig. 11a). Mean 2-m air temperatures are cooler over the whole domain in NYHOPS-SST, with large overwater areas displaying >1°C cooler air, as compared with CONTROL-SST, and with large overland regions showing approximately 0.25°C cooler air (Figs. 11c,d). The area of the largest model differences now extends farther offshore than during the southerly wind regime in Fig. 7b. During upwelling-favorable winds, the roughness of the urban area may reduce the inland penetration of cool SST effects, for example, in Fig. 7b Manhattan experiences no wind speed reduction in NYHOPS-SST relative to CONTROL-SST; however, during offshore flow, the smooth ocean surface likely facilitates stronger downwind penetration of SST effects. For example, most of western Long Island now has >0.25°C cooler air in NYHOPS-SST (Fig. 11d), in contrast to the upwelling regime of Fig. 8b.

At ALSN6 during the late afternoon and evening, the air warms in both the observational and model time series (Fig. 11b), consistent with offshore flow from warmer land located to the northwest; this will be explored below in this section. The cooler air temperature in NYHOPS-SST agrees better with observations at the ALSN6, but still is up to 1°C too warm. It is of note that lower-level (<27 m) air temperatures from NYHOPS-SST show even better agreement with the 29-m observed air temperatures at ALSN6 than the 27-m model level. The strong sensitivity to model height may be due to the shallowness of the IBL that forms in NYHOPS-SST, but not in CONTROL-SST; this is also described in detail below.

As surveyed in the introduction, IBLs are prone to develop whenever discontinuous changes in surface features occur. IBL growth processes over water represent a balance between shear-driven mixing of cold air and BL stabilization resulting from surface heat loss

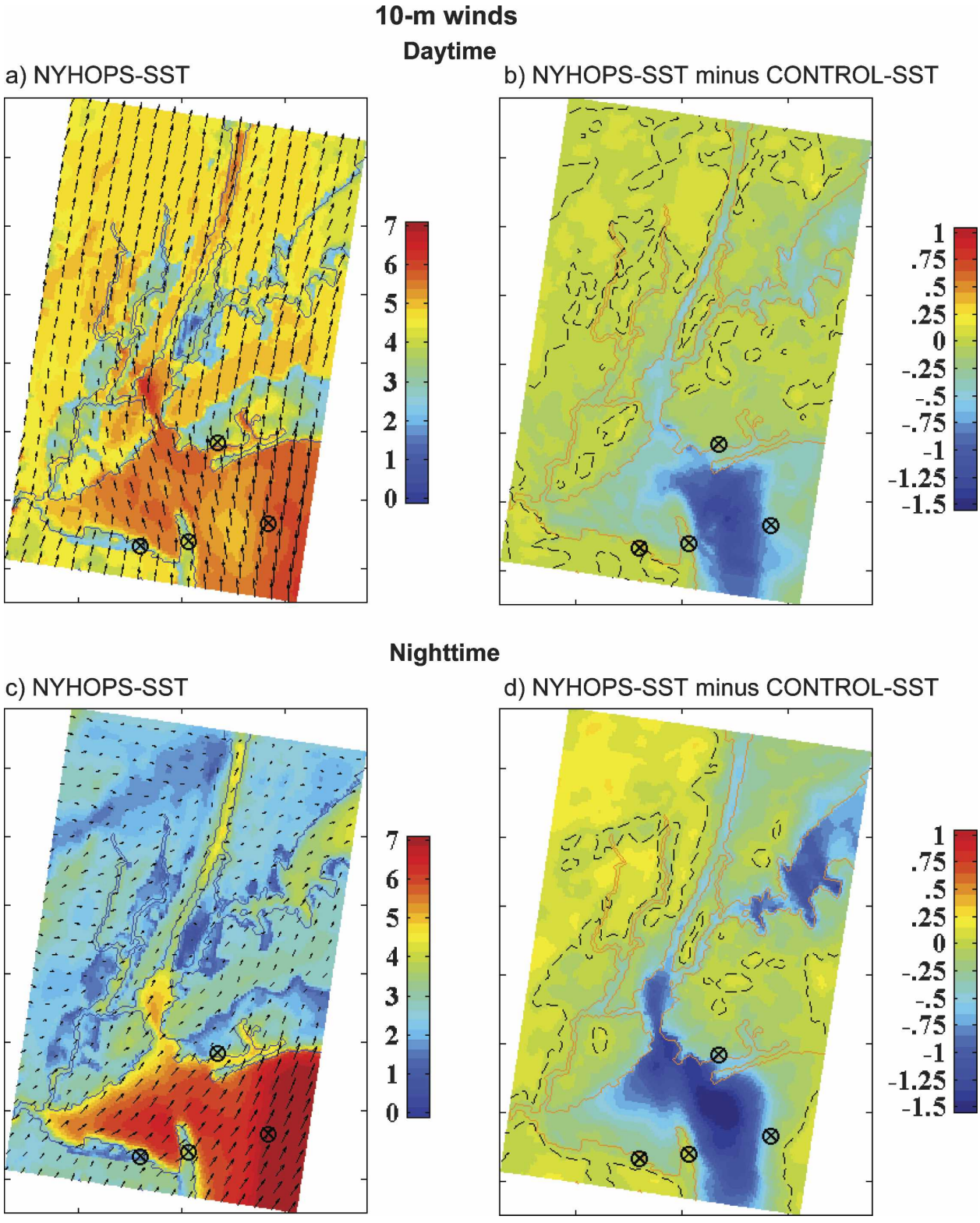


FIG. 9. COAMPS mean 10-m winds (m $s^{-1}$), similar to Fig. 7, but for daytime [1300–0000 UTC (0900–2000 LT)] for (a) NYHOPS-SST and (b) NYHOPS-SST minus CONTROL-SST and nighttime [0100–1200 UTC (2100–0800 LT)] for (c) NYHOPS-SST and (d) NYHOPS-SST minus CONTROL-SST.

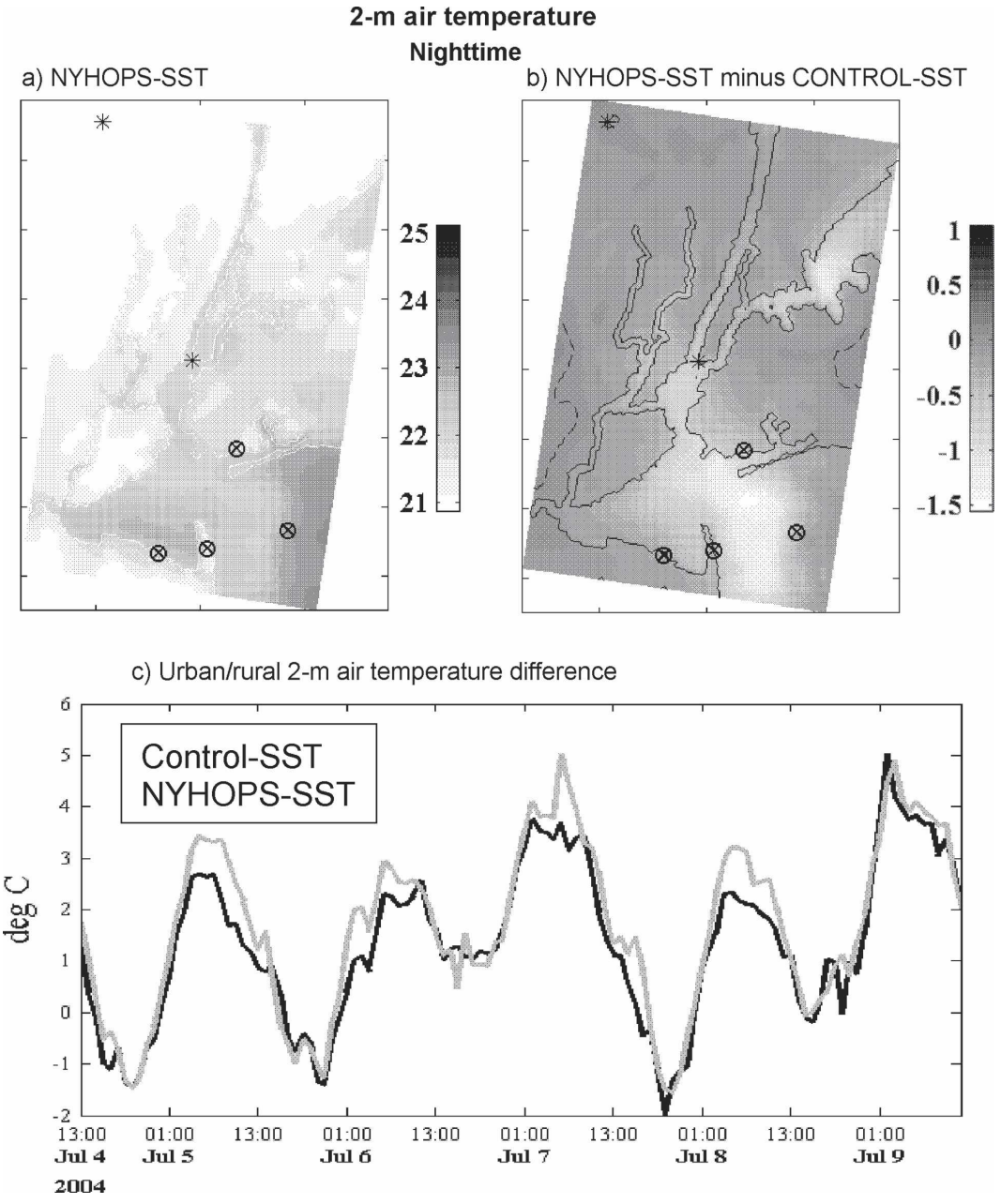


FIG. 10. Mean nighttime 2-m air temperature (°C) for (a) NYHOPS-SST and (b) NYHOPS-SST − CONTROL-SST, and (c) urban–rural temperature difference (°C) for CONTROL-SST (gray) and NYHOPS-SST (black), computed using two points with asterisk in (a) and (b).

(Rogers et al. 1995), that is, increasing stability resulting from surface heat loss promotes shear that leads to enhanced TKE, which causes decreased stability and a deeper BL. In this deeper BL, TKE is reduced and the heat loss again dominates. This process continues until the heat loss goes to zero, and results in a deepening of the IBL downwind. In recent observations, TKE advected from land has been shown to be a factor in IBL dynamics not accounted for in classical theories of IBL development (Vickers and Mahrt 2001). Angevine et al. (2006a) found it to be a dominant feature of IBLs observed off New England, where advected TKE likely supplied the mixing to cool the air column when surface heat fluxes were small.

In NYHOPS-SST, the IBL forms as a direct result of the cooler SSTs in the NY–NJ harbor. The cooler SSTs result in an increased downward heat flux and a cooling of near-surface air temperatures. This induces meso-

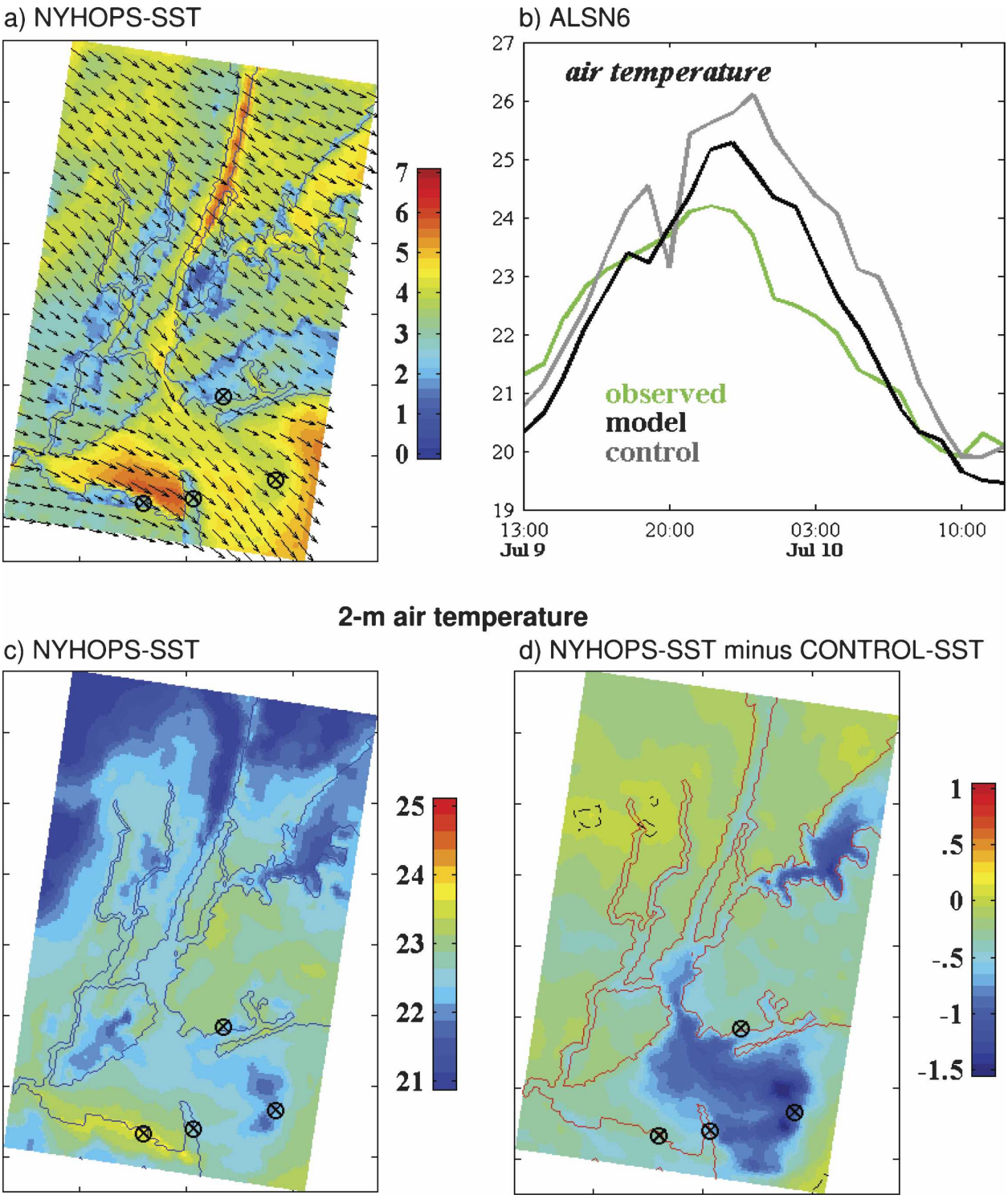


FIG. 11. COAMPS simulations for the 24-h forecast from 1300 UTC 9 Jul to 1200 UTC 10 Jul for (a) NYHOPS-SST mean 10-m winds (m $s^{-1}$); (b) time series of air temperature (°C) at ALSN6 for NYHOPS-SST (black), CONTROL-SST (gray), and observations (green); and mean 2-m air temperature (°C) for (c) NYHOPS-SST and d) NYHOPS-SST minus CONTROL-SST.

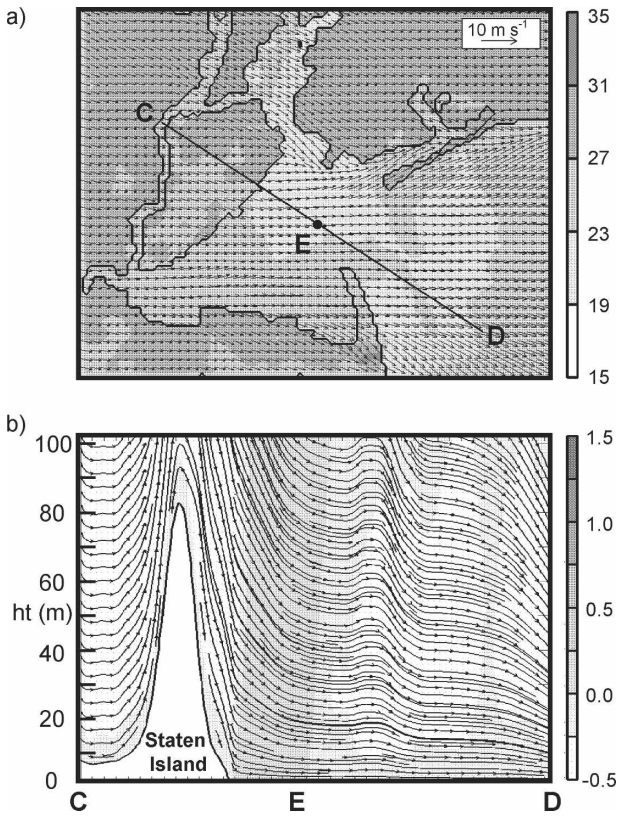


FIG. 12. COAMPS nest-5 3-h forecast valid at 1500 UTC 9 Jul 2004 for NYHOPS-SST simulation for (a) subarea over NY–NJ harbor of surface temperature (ground/SST, shaded, °C) and 10-m winds (every other wind arrow is shown); and b) vertical cross section C–D of gradient Richardson number (shaded) and circulation in plane of cross section.

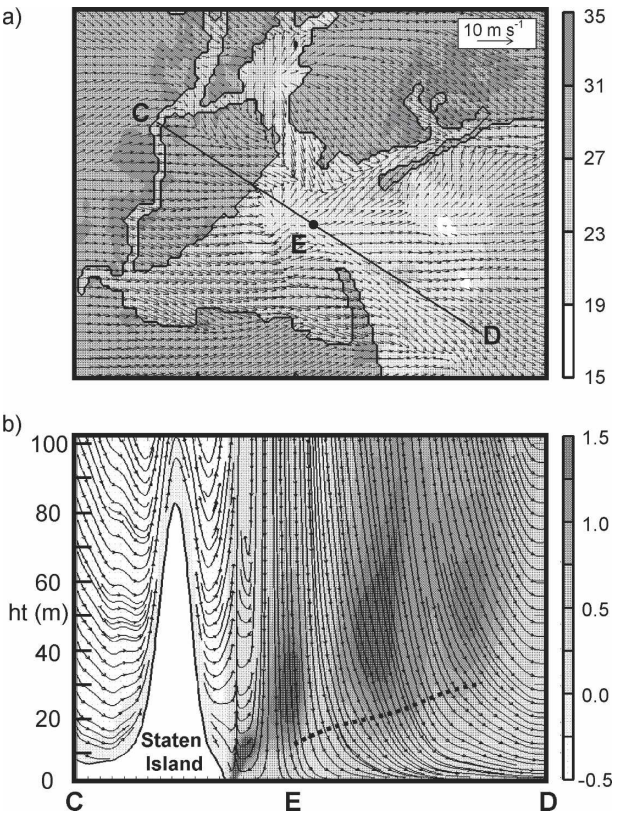


FIG. 13. Same as Fig. 12, but for 6-h forecast valid at 1800 UTC 9 Jul 2004. Dashed line in (b) is the subjectively determined depth of internal boundary layer based on vertical stability gradient.

scale pressure perturbations that result in development of low-level divergence regions over the cooler waters, as clearly illustrated in the temporal IBL evolution shown in Figs. 12 and 13. The low-level flow at 1500 UTC 9 July prior to IBL development is predominately from the west, resulting from the synoptic forcing (Fig. 12a). An onshore component exists near Plumb Beach (Brooklyn) as the sea breeze begins to develop. The vertical (surface to 100 m) cross section along C–D of the gradient Richardson number (Ri) shows near-neutral atmospheric stability in the lower BL that is due to the relatively homogeneous low-level flow (Fig. 12b). By 1800 UTC, the cool pool of low-level air is evident over the cooler SSTs as IBL development begins (Fig. 13a). The regions of cooler SSTs, such as near point E (as well as in the inner harbor just south of Manhattan), clearly show divergent flow. This flow generally opposes the larger-scale westerly flow, resulting in several convergence zones, much like sea-breeze fronts. Along cross section C–D, the developing cool IBL depth remains shallow (generally $<20$ m, as indicated by the dashed line in Fig. 13b) and is moister than the surrounding environment, resulting from latent heat trapping beneath the stable layer (not shown). Limited deepening occurs because of insufficient TKE to provide the necessary vertical mixing. Also, during this preformation period (1500–1800 UTC), the near-surface-based divergence induces downward vertical motion, with values as large as $-0.25$ m s$^{-1}$ at 70-m elevation evident near E (not shown) that serve to inhibit IBL deepening. A minimal downward momentum transport is associated with the subsidence, and the increased TKE does not reach the surface.

The mechanism by which low-level TKE is increased, and by which the IBL initially deepens, is shown in the time–height cross section at point E from 1500 UTC 9 July to 0300 UTC 10 July (Fig. 14). The increase in TKE at 2000 UTC (Fig. 14a) coincides with the initial cooling of the lowest 10s of meters near the surface (Fig. 14b), as well as with an increase in water vapor mixing ratio $q$. The TKE is not locally generated, but clearly is advected from the warmer land to the west

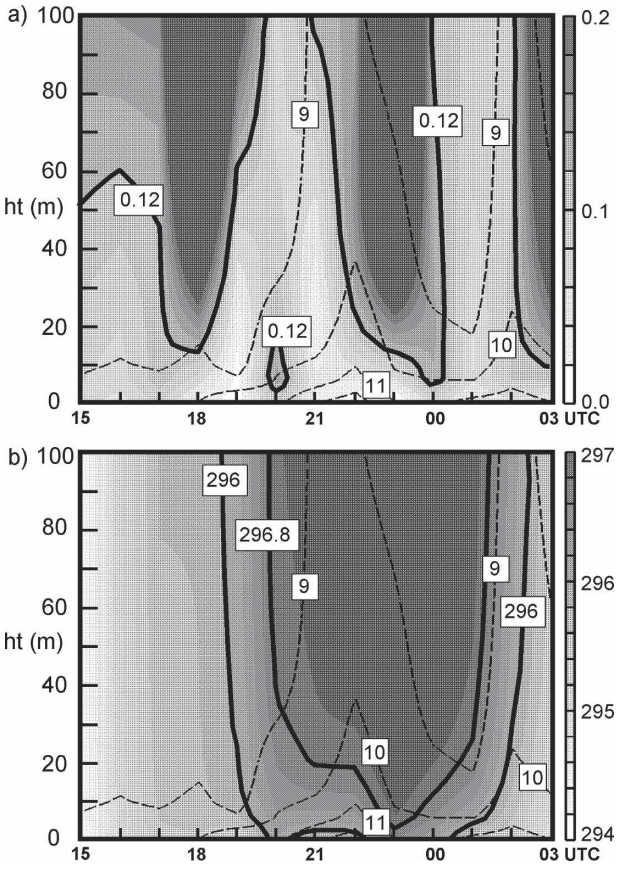


FIG. 14. Time–height cross section for NYHOPS-SST simulation at point E from 1500 UTC 9 Jul to 0300 UTC 10 July for (a) TKE (shaded; $m^2\ s^{-2}$), with 0.12 $m^2\ s^{-2}$ contour in boldface, and mixing ratio (dashed; g $kg^{-1}$) and (b) potential temperature (shaded; K), with the 296.0- and 296.8-K contours in boldface, and mixing ratio (dashed; g $kg^{-1}$).

(Fig. 15). Large TKE values over NJ (south of Staten Island) are advected over warm water and maintain relatively large values (~0.3–0.5 $m^2\ s^{-2}$ near E). As the IBL begins to deepen, TKE is reduced and the heat loss term dominates (Fig. 16), as described in Rogers et al. (1995). The downward sensible heat flux at E is greatest at approximately 2000 UTC and decreases by 2300 UTC (approximately $-3$ W $m^{-2}$), showing that thermally induced IBL deepening is aided by TKE advection. The IBL reaches its maximum depth at approximately 2200 UTC (~40 m at E). This is followed by rapid destruction of the IBL at approximately 2300 UTC 9 July–0000 UTC 10 July in response to strong northwesterly (offshore) flow that reestablishes as land–sea temperature differences decrease.

It is worth noting that the IBL does not form in CONTROL-SST (Fig. 17). When it is deepest in NYHOPS-SST (~2100–2200 UTC), the low-level land–sea temperature difference is much smaller in

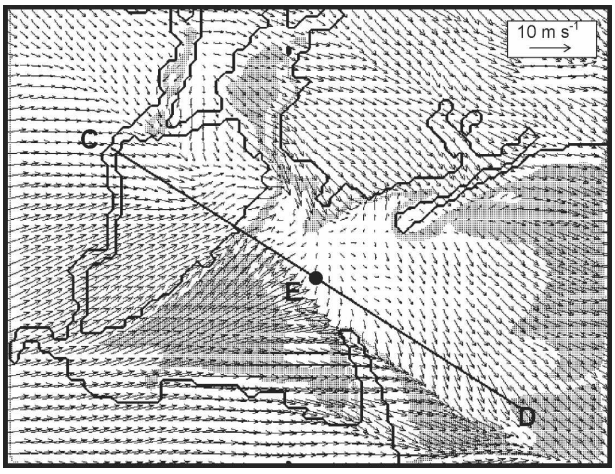


FIG. 15. COAMPS nest-5 7-h forecast valid at 1900 UTC 9 Jul for NYHOPS-SST simulation for subarea over NY–NJ harbor of 27-m-elevation TKE (shaded for $0.1 < \text{TKE} < 0.25$ $m^2\ s^{-2}$) and 27-m winds (every other arrow is shown).

CONTROL-SST (Fig. 17a). Thus, low-level temperatures in CONTROL-SST are relatively horizontally homogeneous and approximately 3°C warmer than NYHOPS-SST (not shown), with a smaller air–sea tem-

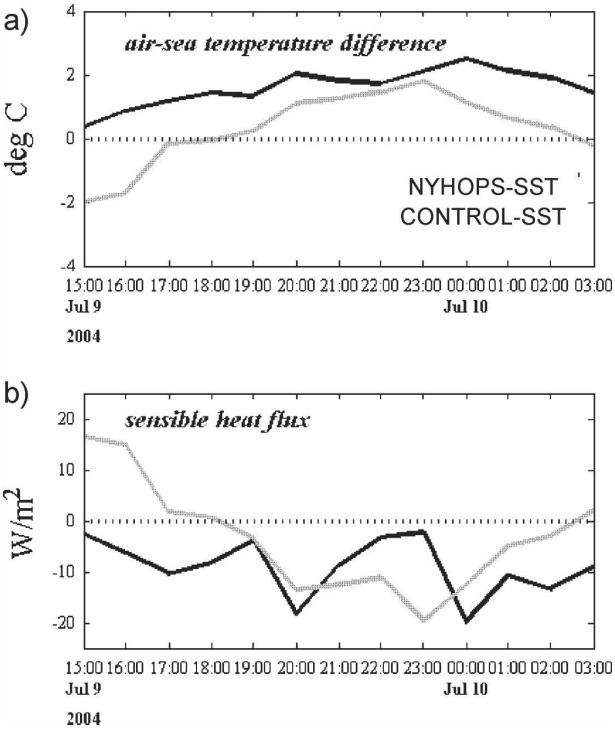


FIG. 16. COAMPS nest-5 time series from 1500 UTC 9 Jul to 0300 UTC 9 Jul at point E for NYHOPS-SST (black) and CONTROL-SST (gray) for (a) air–sea temperature difference (°C) and (b) sensible heat flux (W $m^{-2}$).

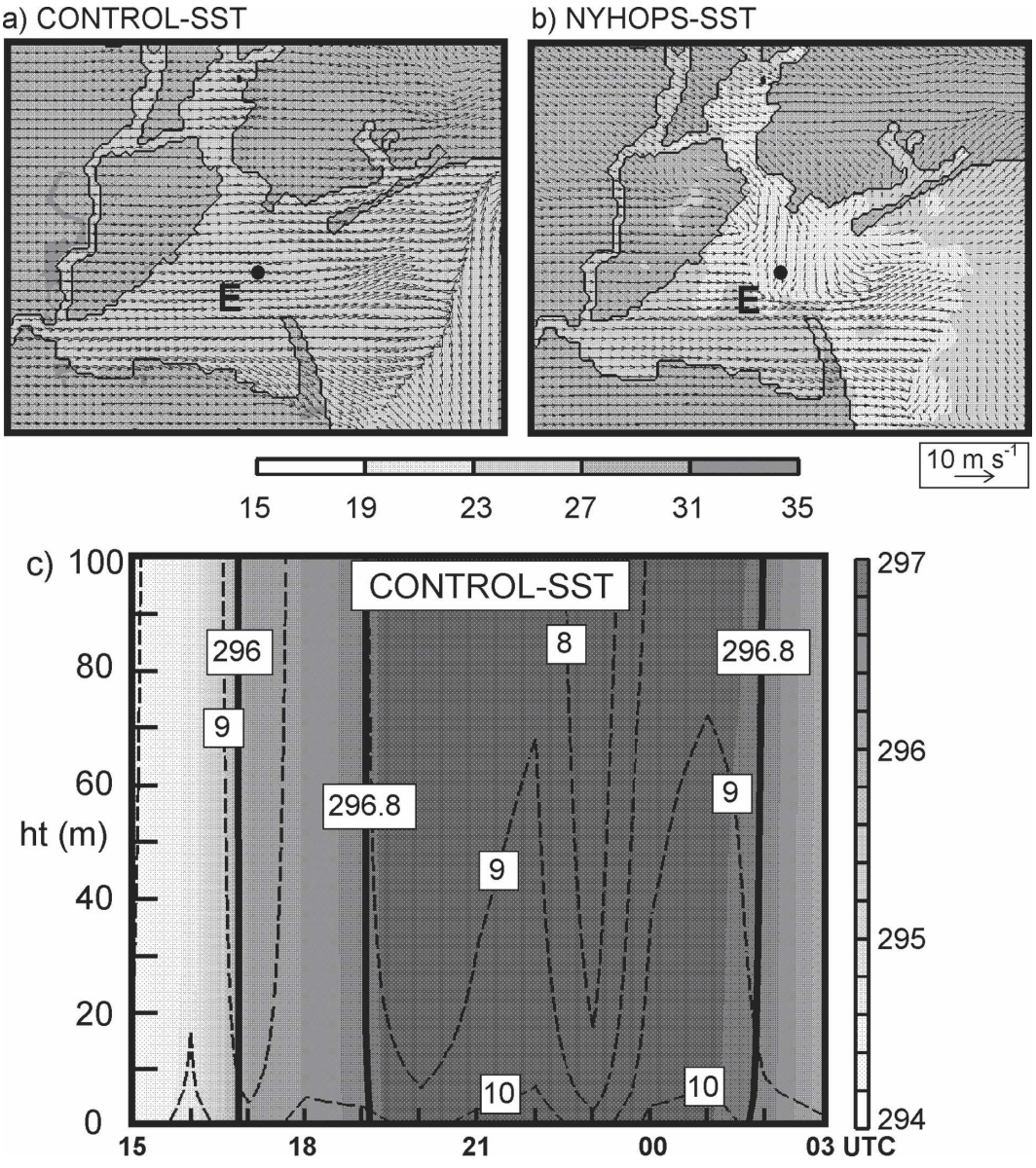


FIG. 17. COAMPS nest 5 for (a) CONTROL-SST 9-h forecast valid at 2100 UTC 9 Jul 2004 for subarea over NY–NJ harbor of surface temperature (ground/SST, shaded, °C) and 10-m winds (every other wind arrow shown); (b) same as (a), but for NYHOPS-SST; (c) CONTROL-SST time–height cross section at point E of potential temperature (shaded; K), with 296.0- and 296.8-K contours in boldface, and mixing ratio (dashed; g kg$^{-1}$), similar to Fig. 14b.

perature difference (Fig. 16a). The lower BL shows near-neutral to slightly unstable low-level stratification (Fig. 17c), in contrast to the cooler IBL evident in NYHOPS-SST (Fig. 14b). The low-level flow remains west-northwesterly for the entire period, with similar warm advection from 2000 to 2300 UTC as that in NYHOPS-SST; however, because of the lack of cooler SSTs, no initial mechanism exists to force IBL development in CONTROL-SST.

Additional differences between the simulations relate to small-scale features in the hourly flow evolution (Figs. 17a,b), with obvious wind direction differences in some areas and with thermally driven local small-scale convergence/divergence features in NYHOPS-SST (Fig. 17b) that are not produced in CONTROL-SST. This is also true (not shown) for those seen in Fig. 13a. Last, winds differ by over 2 m s$^{-1}$ between the simulations in portions of Brooklyn and Manhattan (difference plots are not shown). These simulation differences further demonstrate the important role of local conver-

gence/divergence patterns produced by thermal and roughness contrasts in creating spatial heterogeneity not accounted for in classical IBL theory.

## 6. Discussion and conclusions

The current modeling study is designed to better represent aspects of the mesoscale circulation in the vicinity of the New York–New Jersey harbor. The model thus incorporates an urban canopy parameterization that uses a high-resolution building database and also incorporates hourly high-resolution ocean model–derived SSTs on the innermost two nests of the domain (1.33- and 0.44-km resolution). Results from this high-fidelity SST simulation (NYHOPS-SST) are compared with those from a control simulation (CONTROL-SST) that uses only objectively analyzed SSTs on the innermost nests. Simulations are conducted for the period of 4–11 July 2004 using COAMPS in data assimilation mode.

During generally upwelling-favorable winds in the first 5 days of the simulation, the cold water in NYHOPS-SST cools the overlying air and slows the winds in the mean when compared with CONTROL-SST. In areas over the cold water, 10-m wind speed reductions are 15%–20% and 2-m air temperature reductions are $>1$°C. The effects also extend to the fluctuating fields, as the standard deviations of air temperature and wind speed are also decreased. Both model simulations generally capture important aspects of the flow evolution at the overwater measurement site, including brief frontal passages and weakened winds between these passages. At two land-based and one overwater coastal station, a systematic reduction in wind speed bias exists in NYHOPS-SST. At the overwater ALSN6 light tower site (outside the area of greatest difference between the simulations), a 47.5% (0.38 m $s^{-1}$) reduction in mean bias in NYHOPS-SST is found over CONTROL-SST. As a percentage of the observed value, mean wind speeds are reduced by 6% (from 113% to 107%) at ALSN6, and thus utilization of hourly high-resolution SSTs from NYHOPS led to a somewhat more skillful atmospheric wind speed prediction.

Strong diurnal differences in the atmospheric flow are manifest in both the observations and model simulations. Mean nighttime winds over water are from a more southwesterly orientation in both simulations, when compared with daytime flows. Winds are slowed more at night to a greater degree, and cover a wider area over water, relative to daytime NYHOPS-SST–CONTROL-SST differences. Modeled air temperatures in both simulations at ALSN6 generally agree with the observed warming trend during several nights, except for an event on 6 July resulting from a slight timing error in the predicted frontal passage. The nighttime UHI effect is reduced by over 1°C on three nights in NYHOPS-SST when compared with CONTROL-SST. This has potential implications for forecasting extreme heat events, which are typically exacerbated by UHIs. The repeated experience of elevated temperature and humidity levels over several nights is important in heat-related deaths (Kalkstein 1991). The local cooling effect of upwelled coastal water constitutes a mitigating factor in the nocturnal evolution of the UHI that has previously not been incorporated in simulations of the New York–New Jersey area.

Over a daylong northwesterly flow event on 9–10 July, when cold water has a more pronounced effect on air properties to the east, the mean observed ALSN6 air temperature is 22.13°C, versus 22.30°C in NYHOPS-SST and 23.02°C in CONTROL-SST. The slightly enhanced agreement in NYHOPS-SST is attributed to the formation of a shallow IBL, facilitated by TKE advection from the shore. In the offshore region of small sensible heat flux, moisture flux is trapped and the air cools more than in CONTROL-SST. The feature lasts about 6 h and produces starkly different BL structures in the two simulations. Having observed IBL formation associated with TKE advection from land, Angevine et al. (2006b) attempted to simulate these processes off New England, but their simulations were not able to produce the observed highly stable overwater atmospheric conditions favorable to IBL formation. They used a 2.5-km-resolution COAMPS grid with coarse-resolution (0.5°) daily SST analyses. The current results suggest that the lack of resolution in SST fields may be a factor (along with previously identified insufficient model resolution and too strong mixing) in the inability of that modeling study to capture key aspects of IBL formation.

This study has thus shown that for a localized domain with a high-resolution grid, important atmospheric variables are extremely sensitive to SST specification. In mean statistics presented here, air temperature and wind speed effects resulting from the realistic NYHOPS-SSTs are often confined to overwater areas, and to land areas immediately adjacent to water in the upwelling regime, although mean differences did extend farther over land during the offshore flow regime. In the hourly flow evolution, frequently times exist when there are dramatically different forecasts produced in NYHOPS-SST versus CONTROL-SST. The tendency for the two model simulations to present small-scale differences in forecasts is especially pronounced during transitions between flow regimes. This

holds significance for short-term forecasting of wind speed and direction for critical applications, like contaminant dispersion prediction.

*Acknowledgments.* We are grateful to Jay Titlow of Weatherflow, Inc., for supplying the observations at Plumb Beach and Sandy Hook. Dov Kruger and Shenjun Fan of Stevens Institute of Technology generously provided NYHOPS support and access to evaluation data. We also thank Scott Glenn and the Rutgers University Coastal Ocean Observation Laboratory's Operations Center for processing the satellite AVHRR image and Steve Burian for assembling the New York–New Jersey building database. We benefited from interactions with William Thompson, Michael Brown, Brian Colle, Jerry Allwine, Wayne Angevine, and Michael Tjernstrom. The Department of Homeland Security Urban Dispersion Program supported this work through Grants P4CF40592 and P5CH40318 (J. Pullen and T. Holt), P5CH40321 and P4CH40585 (A. Blumberg), and P4CH0586 and P5CH40382 (R. Bornstein).

## REFERENCES

Angevine, W. M., J. E. Hare, C. W. Fairall, D. E. Wolfe, R. J. Hill, W. A. Brewer, and A. B. White, 2006a: Structure and formation of the highly stable marine boundary layer over the Gulf of Maine. *J. Geophys. Res.,* **111,** D23S22, doi:10.1029/2006JD007465.

——, M. Tjernstrom, and M. Zagar, 2006b: Modeling of the coastal boundary layer and pollutant transport in New England. *J. Appl. Meteor. Climatol.,* **45,** 137–154.

Bane, J. M., M. D. Levine, R. M. Samelson, S. M. Haines, M. F. Meaux, N. Perlin, P. M. Kosro, and T. Boyd, 2005: Atmospheric forcing of the Oregon coastal ocean during the 2001 upwelling season. *J. Geophys. Res.,* **110,** C10S02, doi:10.1029/2004JC002653.

Blumberg, A. F., and G. L. Mellor, 1987: A description of a three-dimensional coastal ocean circulation model. *Three-Dimensional Coastal Ocean Models,* N. S. Heaps, Ed., Amer. Geophys. Union, 1–16.

——, and F. L. Hellweger, 2006: Hydrodynamics of the Hudson River Estuary. *Hudson River Fishes and their Environment,* J. Waldman, K. Limburg, and D. Strayer, Eds., American Fisheries Society, 9–28.

——, L. A. Khan, and J. P. St. John, 1999: Three-dimensional hydrodynamic model of New York Harbor region. *J. Hydraul. Eng.,* **125,** 799–816.

Bornstein, R. D., 1968: Observations of the urban heat island effect in New York City. *J. Appl. Meteor.,* **7,** 575–582.

——, and D. S. Johnson, 1977: Urban-rural wind velocity differences. *Atmos. Environ.,* **11,** 597–604.

——, and W. T. Thompson, 1981: Effects of frictionally retarded sea breeze and synoptic frontal passages on sulfur dioxide concentrations in New York City. *J. Appl. Meteor.,* **20,** 843–858.

Bornstein, R., and M. LeRoy, 1990: Urban barrier effects on convective and frontal thunderstorms. Preprints, *Fourth Conf. on Mesoscale Processes,* Boulder, CO, Amer. Meteor. Soc., 25–29.

Brown, M. J., and M. Williams, 1998: An urban canopy parameterization for mesoscale meteorological models. *Proc. Second Symp. on the Urban Environment,* Albuquerque, NM, Amer. Meteor. Soc., 144–147.

Bruno, M. S., and A. F. Blumberg, 2004: An urban ocean observatory for the maritime community. *Sea Technol.,* **45,** 27–32.

Burian, S. J., A. McKinnon, J. Hartman, and W. Han, 2005: Gridded building statistics for New York City. Final Rep. for Los Alamos National Laboratory, DHS NYC Dispersion Project, 16 pp.

Chelton, D. B., and Coauthors, 2001: Observations of coupling between surface wind stress and sea surface temperature in the eastern tropical Pacific. *J. Climate,* **14,** 1479–1495.

——, M. G. Schlax, M. H. Freilich, and R. F. Milliff, 2004: Satellite measurements reveal persistent small-scale features in ocean winds. *Science,* **303,** 978–983.

Chen, S., and Coauthors, 2003: COAMPS™ version 3 model description. Naval Research Laboratory, Marine Meteorology Division, 143 pp.

Chin, H.-N. S., M. J. Leach, G. A. Sugiyama, J. M. Leone Jr., H. Walker, J. S. Nasstrom, and M. J. Brown, 2005: Evaluation of an urban canopy parameterization in a mesoscale model using VTMX and URBAN 2000 data. *Mon. Wea. Rev.,* **133,** 2043–2068.

Fan, S., A. F. Blumberg, M. S. Bruno, D. Kruger, and B. Fullerton, 2006: The skill of an urban ocean forecast system. *Estuarine and Coastal Modeling,* M. L. Spaulding, Ed., ASCE, 603–618.

Garratt, J. R., 1990: The internal boundary layer—A review. *Bound.-Layer Meteor.,* **50,** 171–203.

Gedzelman, S. D., S. Austin, R. Cermak, N. Stefano, S. Partridge, S. Quesenberry, and D. A. Robinson, 2003: Mesoscale aspects of the Urban Heat Island around New York City. *Theor. Appl. Climatol.,* **75,** 29–42.

Glenn, S., and Coauthors, 2004: Biogeochemical impact of summertime coastal upwelling on the New Jersey Shelf. *J. Geophys. Res.,* **109,** C12S02, doi:10.1029/2003JC002265.

Harshvardhan, R. Davies, D. A. Randall, and T. G. Corsetti, 1987: A fast radiation parameterization for atmospheric circulation models. *J. Geophys. Res.,* **92,** 1009–1016.

Hodur, R. M., 1997: The Naval Research Laboratory's Coupled Ocean/Atmosphere Mesoscale Prediction System (COAMPS). *Mon. Wea. Rev.,* **125,** 1414–1430.

Holt, T., and J. Pullen, 2007: Urban canopy modeling of the New York City metropolitan area: A comparison and validation of single- and multilayer parameterizations. *Mon. Wea. Rev.,* **135,** 1906–1930.

Kain, J. S., and J. M. Fritsch, 1993: Convective parameterization for mesoscale models: The Kain–Fritsch scheme. *The Representation of Cumulus Convection in Numerical Models, Meteor. Monogr.,* No. 24, Amer. Meteor. Soc., 165–170.

Kalkstein, L. S., 1991: The potential impact of climate upon human mortality. *Environ. Health Perspect.,* **96,** 145–150.

Khairoutdinov, M., and Y. Kogan, 2000: A new cloud physics parameterization in a large eddy simulation model of marine stratocumulus. *Mon. Wea. Rev.,* **128,** 229–243.

Loose, T., and R. D. Bornstein, 1977: Observations of mesoscale effects on frontal movement through an urban area. *Mon. Wea. Rev.,* **105,** 563–571.

Louis, J.-F., M. Tiedtke, and J. F. Geleyn, 1982: A short history of the operational PBL-parameterization of ECMWF. *Workshop on Planetary Boundary Layer Parameterization,* Reading, United Kingdom, European Centre for Medium-Range Weather Forecasts, 59–79.

Mellor, G. L., and T. Yamada, 1982: Development of a turbulence closure model for geophysical fluid problems. *Rev. Geophys.,* **20,** 851–875.

Neuman, M., 1996: Evidence of upwelling along the New Jersey coastline and the south shore of Long Island, New York. *Bull. Nat. J. Acad. Sci.,* **41,** 7–13.

Novak, D. R., and B. A. Colle, 2006: Observations of multiple sea breeze boundaries during an unseasonably warm day in metropolitan New York City. *Bull. Amer. Meteor. Soc.,* **87,** 169–174.

Oke, T. R., and G. B. Maxwell, 1975: Urban heat island dynamics in Montreal and Vancouver. *Atmos. Environ.,* **9,** 191–200.

Rogers, D. P., D. W. Johnson, and C. A. Friehe, 1995: The stable internal boundary layer over a coastal sea. Part I: Airborne measurements of the mean and turbulence structure. *J. Atmos. Sci.,* **52,** 667–683.

Rutledge, S. A., and P. V. Hobbs, 1983: The mesoscale and microscale structure and organization of clouds and precipitation in midlatitude cyclones. VIII: A model for the "seeder-feeder" process in warm-frontal rainbands. *J. Atmos. Sci.,* **40,** 1185–1206.

Skyllingstad, E. D., R. M. Samelson, L. Mahrt, and P. Barbour, 2005: A numerical modeling study of warm offshore flow over cool water. *Mon. Wea. Rev.,* **133,** 345–361.

Smedman, A.-S., H. Bergstrom, and B. Grisogono, 1997: Evolution of stable internal boundary layers over a cold sea. *J. Geophys. Res.,* **102,** 1091–1099.

Song, Y. T., D. B. Haidvogel, and S. M. Glenn, 2001: Effects of topographic variability on the formation of upwelling centers off New Jersey: A theoretical model. *J. Geophys. Res.,* **106,** 9223–9240.

Vickers, D., and L. Mahrt, 2001: Structure of offshore flow. *Mon. Wea. Rev.,* **129,** 1251–1258.

——, and ——, 2004: Atmospheric response to sea-surface temperature variability. Preprints, *13th Conf. on Interactions of the Sea and Atmosphere,* Portland, ME, Amer. Meteor. Soc., CD-ROM, 2.9.